Available online at www.sciencedirect.com
SCIENCE DIRECT®
Journal of Power Sources 128 (2004) 308–318
JOURNAL OF POWER SOURCES
www.elsevier.com/locate/jpowsour

Thermal abuse performance of high-power 18650 Li-ion cells

E.P. Roth*, D.H. Doughty

Lithium Battery R&D Department, Sandia National Laboratories, Albuquerque, NM 87185, USA

Received 12 September 2003; accepted 27 September 2003

Abstract

High-power 18650 Li-ion cells have been developed for hybrid electric vehicle applications as part of the DOE Advanced Technology Development (ATD) program. The thermal abuse response of two advanced chemistries (Gen1 and Gen2) were measured and compared with commercial Sony 18650 cells. Gen1 cells consisted of an MCMB graphite based anode and a $LiNi_{0.85}Co_{0.15}O_2$ cathode material while the Gen2 cells consisted of a MAG10 anode graphite and a $LiNi_{0.80}Co_{0.15}$ $Al_{0.05}O_2$ cathode. Accelerating rate calorimetry (ARC) and differential scanning calorimetry (DSC) were used to measure the thermal response and properties of the cells and cell materials up to 400 °C. The MCMB graphite was found to result in increased thermal stability of the cells due to more effective solid electrolyte interface (SEI) formation. The Al stabilized cathodes were seen to have higher peak reaction temperatures that also gave improved cell thermal response. The effects of accelerated aging on cell properties were also determined. Aging resulted in improved cell thermal stability with the anodes showing a rapid reduction in exothermic reactions while the cathodes only showed reduced reactions after more extended aging. Published by Elsevier B.V.

Keywords: Li-ion battery; Thermal abuse; ARC; DSC; $LiNi_{0.85}Co_{0.15}O_2$; $LiNi_{0.80}Co_{0.15}$ $Al_{0.05}O_2$

1. Introduction

The Advanced Technology Development (ATD) Program was established by DOE to assist the partnership for a new generation of vehicles (PNGV) industrial developers of high-power lithium-ion batteries to overcome key barriers in the areas of abuse tolerance, calendar life, and cell packaging cost. One goal of this project is to rapidly develop high-power lithium-ion cell chemistries, using commercially available materials that can be shared with the industrial battery developers. A second goal is to establish the performance, life, and thermal abuse characteristics of these cells. Abuse tolerance has been a major concern limiting the application of advanced Li-ion chemistries in the consumer market. Abuse can be categorized as physical abuse (crush, nail penetration), electrical abuse (short circuit, overcharge) and thermal abuse (overheating, thermal runaway). Thermal abuse can result from relatively normal operating conditions where the heat generation rate of the cells exceeds the heat removal from the battery system. Cell thermal runaway has been described by other researchers [1–3] and found to be sensitive to the particular cell chemistry and operating conditions such as state of charge (SOC) and history.

In order to study the technical barriers of abuse tolerance, it is necessary to have detailed knowledge about the cell chemistry and the cell performance under a wide range of abusive conditions. The mechanisms leading to poor abuse tolerance need to be understood to allow development of advanced cell chemistries which meet all the requirements for performance, life, cost, and safety. The Thermal Abuse Tolerance Program at Sandia has concentrated on studying the behavior of cells and cell materials that have been specifically designed to meet these safety and power requirements. Two generations of cell chemistries (Gen1 and Gen2) were specified and manufactured to allow detailed study and comparison of lifetime, performance, and safety. The cell chemistries were chosen to best meet the program performance requirements after screening numerous commercially available material combinations by program partners at Argonne National Laboratory. The 18650 cell configuration was chosen to allow quick and economical cell manufacture in a meaningful cell size. The thermal response of these high-power cells was compared to commercial Sony 18650 cells under similar operating conditions.

Thermal abuse tolerance was studied using calorimetric techniques on full cells and on cell components. Accelerating rate calorimetry (ARC) was used to measure the thermal runaway response of full cells at increasing SOC for both fresh cells and cells that had undergone high temperature aging. Differential scanning calorimetry (DSC)

* Corresponding author. Tel.: +1-505-844-3949; fax: +1-505-844-6972.
E-mail address: eproth@sandia.gov (E.P. Roth).

0378-7753/$ – see front matter Published by Elsevier B.V.
doi:10.1016/j.jpowsour.2003.09.068

was also used to compare the thermal response of the cell components.

2. Experimental

2.1. Cell composition

The Gen1 cells were constructed using $LiNi_{0.85}Co_{0.15}O_2$ cathode (Sumitomo) active material and MCMB 6-2800 graphite (Osaka Gas) as the active anode material. The cathode also included carbon black (Chevron) and SFG-6 (Timcal) graphite for conductivity enhancement with PVDF (Kureha KF-1100) as the binder. The anode material included SFG-6 graphite and the PVDF binder. The mass compositions of the films are given in Table 1. The electrolyte consisted of 1 M $LiPF_6$ in ethylene carbonate: diethyl carbonate (EC:DEC 1:1). The cells were manufactured by PolyStor [4] using a negative steel case design with a crimped seal configuration. The nominal cell capacity was 0.9 Ah.

The Gen2 cell chemistry was chosen based on the performance of the Gen1 cells. The Gen2 cathode consisted of $LiNi_{0.8}Co_{0.15}Al_{0.05}O_2$ (Fuji CA1505), which was chosen for its enhanced thermal stability. The cathode also included the carbon black and SFG-6 with PVDF binder. The anode consisted of a flaky carbon MAG-10 (Hitachi Chemical) and PVDF binder. Table 1 again lists the compositions. The electrolyte consisted of 1.2 M $LiPF_6$ in ethylene carbonate:ethyl methyl carbonate (EC:EMC 3:7). The Gen2 cells were manufactured by Quallion [5] using a laser-welded positive Al case design with a machined vent. The nominal Gen2 capacity was 1.0 Ah. Commercial Sony Li-ion 18650 cells (US18650S STG) were also measured to allow a comparison to known cell performances.

2.2. Cell conditioning

All cells underwent initial cycling characterizations including five *C*/1 charge/discharge cycles between 3.0 and 4.1 V followed by a *C*/10 cycle for determination of capacity. Cycling was performed using a Maccor Battery Cycler with the cells in a thermal block to limit temperature excursions. The Gen2 cells were also aged at elevated temperatures (25, 35, 45 and 55 °C) and states of charge (60, 80 and 100%) for increasing periods of time as part of an accelerated life test (ALT) study. Calorimetric measurements were made on selected cells to determine the main effects of this aging.

2.3. Calorimetric techniques

ARC testing was performed on full cells at increasing states of charge and after high-temperature aging. A maximum temperature of 160 °C was set to prevent uncontrolled thermal runaway and explosive decomposition of the cells in the ARC apparatus (Arthur D. Little Model 2000, AD Little, Acorn Park, Cambridge, MA). The ARC was operated in a heat, wait, search mode to allow determination of the onset of self-heating. The ARC increases the temperature in discrete steps, waits for the thermal transients to decay and then monitors the temperature of the cell for a fixed time period. If the cell temperature is not increasing above a threshold value, typically 0.02 °C/min, the temperature is increased by another step and the process repeated. If the cell temperature increases at rate equal or above the threshold value, the ARC switches to the exotherm mode during which the ARC temperature closely matches the cell temperature, thus maintaining the adiabatic state. The ARC matches the rate of temperature rise of the cell even at quite high heating rates. The normal mode of operation of the ARC terminates an experiment by cooling the sample once it reaches a set upper temperature limit. The ARC experiment closely simulates a thermal abuse environment that includes moderately high temperatures for relatively long periods of time.

DSC measurements were performed using a TA Instruments Model 2910 (TA Instruments, New Castle, DE). DSC runs were performed using crimped Al pans prepared in an Argon glove box. The measured temperature range was from 0 to 400 °C. The amount of material was minimized to reduce gas evolution at higher temperatures. Even so, Al pans usually vented at temperatures above 250 °C with

Table 1
Cell chemistries and electrode compositions

Sony cells (commercial)	Anode/cathode/electrolyte	Coke-based carbon + unknown $LiCoO_2$ + unknown PC:DMC/$LiPF_6$
Gen1 cells (Argonne National Laboratory design)	Anode	75% MCMB-6-2800 carbon, 16% SFG-6 graphite, 9% PVDF binder
	Cathode	84% $LiNi_{0.85}Co_{0.15}O_2$, 4% carbon black, 4% SFG6 graphite, 8% PVDF binder
	Electrolyte	1 M $LiPF_6$ in EC:DEC (1:1)
Gen2 cells (Argonne National Laboratory design)	Anode	92% MAG10 graphite, 8% PVDF binder
	Cathode	84% $LiNi_{0.80}Co_{0.15}Al_{.05}O_2$, 4% carbon black, 4% SFG6 graphite, 8% PVDF binder
	Electrolyte	1.2 M $LiPF_6$ in EC:EMC (3:7)

an accompanying endothermic peak in the measured signal. Hermetic, high-pressure steel pans were also used which contained the evolved gases but these pans have high mass and are less sensitive to low thermal events compared to the Al pans. The appropriate pan was used to give the greatest sensitivity in the region of interest. A scan rate of 10 °C/min was used for the low-mass Al pans and 5 °C/min for the higher mass hermetic steel pans.

3. Results and discussion

3.1. ARC runs

3.1.1. Sony cells

Initial ARC runs were performed for the "as received" Sony cells from 0 to 100% SOC as shown in Fig. 1. These cells were measured in an open cell holder configuration. The onset temperature of self-generated heating decreased with increasing SOC while the magnitude of the self-generated heating rate at a given temperature increased. Fig. 2 shows the ARC data vertically offset for easier comparison along with the measured cell voltages. The heating rates are only shown for the exothermic regions where self heating was above 0.02 °C/min. Self-generated heating occurred as low as 50 °C, but accelerating heating rate was not observed until above 100 °C. At 100 °C, a sharp increase in the heating rate was observed for cells at 50% SOC or greater. A "knee" in the heating rate around 110 °C has been associated with breakdown of the anode solid electrolyte interface (SEI) layer followed by exothermic reduction of the electrolyte by the lithiated carbon [6,7]. The increase of this reaction with increasing SOC indicates only a moderately effective SEI layer. A dip in the heating rate around 125 °C resulted from the endothermic melting of the polyethylene separator material which was also indicated by the sudden

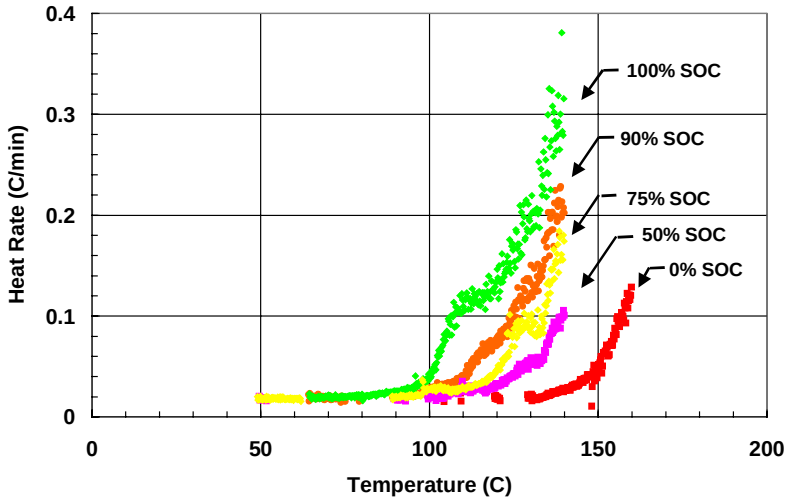

Fig. 1. ARC data for Sony cells from 0 to 100% SOC.

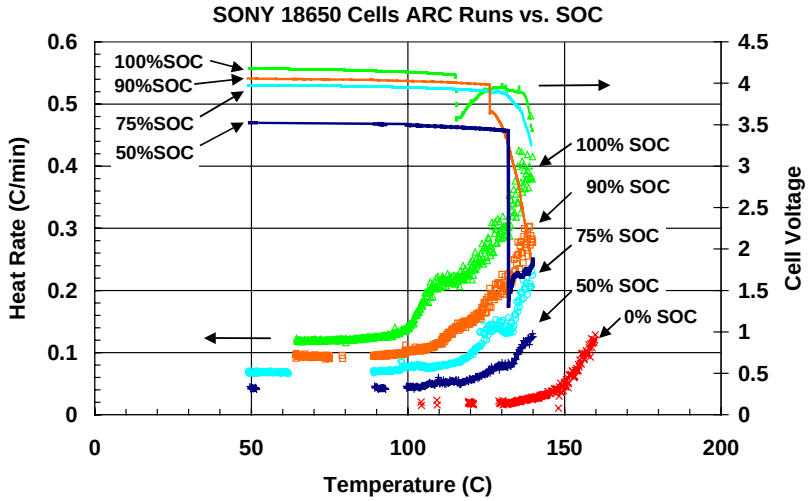

Fig. 2. ARC data for Sony cells from 0 to 100% SOC (vertically offset) showing onset of self-generated heating along with cell voltages.

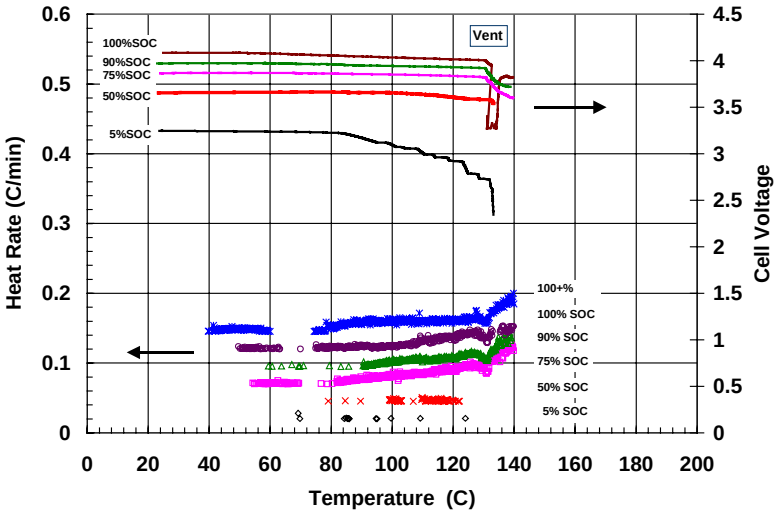

Fig. 3. ARC data for Gen1 cells from 0 to 100% SOC (vertically offset) showing onset of self-generated heating along with cell voltages.

drop in cell voltage at those temperatures. In addition, cell venting often occurred slightly above this temperature with resultant transient cooling of the cell. Cell voltage drops were seen around 125 °C corresponding to the separator melt temperature and the resulting large increase in cell impedance. The voltage drops did not result from internal shorting of the cells since no sudden increase in heating rate was observed. These initial ARC runs limited the maximum temperature to 140 °C (160 °C for the 0% SOC cell) to prevent uncontrolled, explosive decomposition of the cell in the ARC chamber. Previous work has shown that the cells go into uncontrolled thermal runaway around 180 °C [1,8].

3.1.2. Gen1 cells

ARC runs were performed on Gen1 cells at several SOCs while monitoring the cell voltages. The maximum temperature was again set at 140 °C. The ARC data, vertically offset in Fig. 3, show that the Gen1 cells have greater thermal stability than seen for the commercial Sony cells. The cells with 50% or lower SOC showed no accelerated heating, only transient heating spikes. The cells with higher SOC showed a low-temperature constant heating rate whose onset temperature decreased with increasing SOC to as low as 40 °C. Sustained heating only occurred above 80 °C. Low-level heating rates were observed up to 130 °C at which point separator melt occurred with a resultant dip in the heating rate. Above this temperature, the heating rate began to accelerate until termination of the measurement. The magnitudes of the heating rates were similar for all of the SOCs indicating a well-developed SEI layer. Cell voltages dropped upon separator melting but no discontinuities in the heating rate were observed indicating that no short circuits occurred within the cell.

The Sony and Gen1 ARC behaviors at 100% SOC are compared in Fig. 4 up to a temperature limit of 160 °C. The Sony cell vented at 140 °C while the Gen1 cell remained sealed. Venting resulted in more erratic heating rates in the cell due to the cooling effects of the released gas. The Gen1 cell had significantly improved thermal stability compared to the Sony cell over this whole temperature range.

3.1.3. Gen2 cells

The Gen2 cells were likewise measured at increasing states of charge (60 and 100% SOC). Fig. 5 shows that sustained heating occurred as low as 50 °C at both SOCs. Slightly increased heating rates were seen for the 100% SOC cell, which then showed more accelerated heating above 115 °C. The Gen2 cells also showed the endotherm at 125 °C resulting from separator melt, at which temperature the cell voltages dropped sharply. Neither of these cells vented up to the temperature limit of 160 °C and neither cell showed any sign of internal short circuit.

The ARC runs for the Sony, Gen1 and Gen2 cells are compared in Fig. 6. The Gen2 cells closely matched the performance of the Sony cells except at the lower temperatures. The Gen2 cells showed continuous, accelerated heating starting below 50 °C with no indication of an abrupt SEI decomposition as seen in the Sony cells. The Gen1 cells

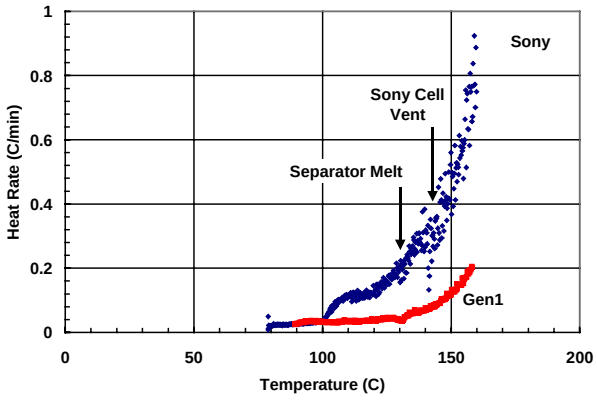

Fig. 4. Comparison of ARC data for Sony and Gen1 cells at 100% SOC.

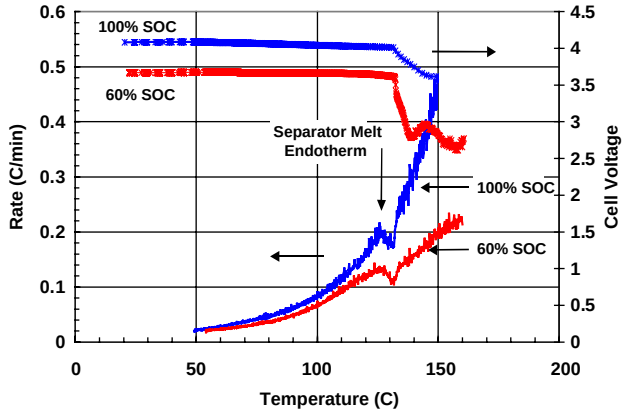

Fig. 5. ARC data for Gen2 cells at 60% SOC and 100% SOC.

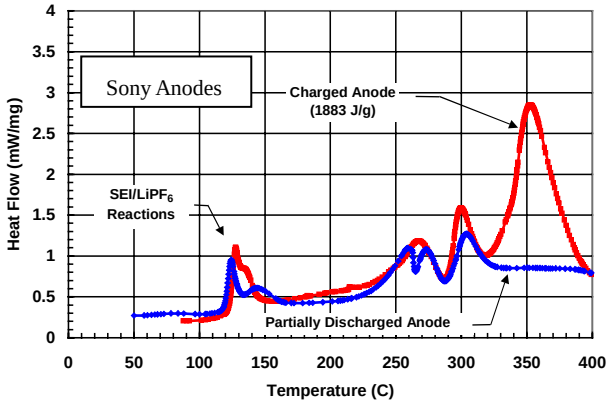

Fig. 7. DSC profiles of charged and discharged Sony anodes in electrolyte.

showed the greatest thermal stability indicating the presence of a very effective anode SEI layer.

3.2. DSC measurements

Electrode materials were removed from selected cells of each cell type for comparative DSC analysis in both charged and discharged states. The charge state of the nominally discharged Sony cell material was less than 50% SOC but not accurately known resulting from the partial discharge of the electrodes during disassembly. All cell materials were measured in the presence of their respective cell electrolytes.

3.2.1. Sony cells

The Sony charged and partially discharged anode materials showed a sharp exothermic decomposition starting at 120 °C as shown in Fig. 7. The onset temperature and peak reaction was independent of the state of charge. This reaction has been identified as resulting from decomposition of the metastable SEI layer [6,7]. The reactions peaks in the 250–300 °C range resulted from electrolyte reduction through the reacting SEI layer followed by strong reaction above 300 °C. This high temperature peak may result from reaction of the lithiated carbon with the binder material (Sony binder unknown) or possibly with some other additive component introduced by the manufacturer. The partially discharged anode material did not show the high-temperature reaction indicating that some Li may have been consumed during the lower temperature reactions resulting in a reduced Li level for the high temperature reaction.

The Sony cathodes showed a strong dependence on SOC as shown in Fig. 8. Reaction peaks were seen in the 200–300 °C range for this $LiCoO_2$ material with a strong peak at 225 °C for the fully charged material [9–11]. Fig. 9 compares the anode and cathode materials and shows that the sequence of thermal reactions starts with low-rate reactions at the anode followed by high-rate reaction peaks at the cathode and then at the anode.

3.2.2. Gen1 cells

Gen1 electrode materials were removed from cells at 100% SOC and 0% SOC and measured in the 1.0 M $LiPF_6$

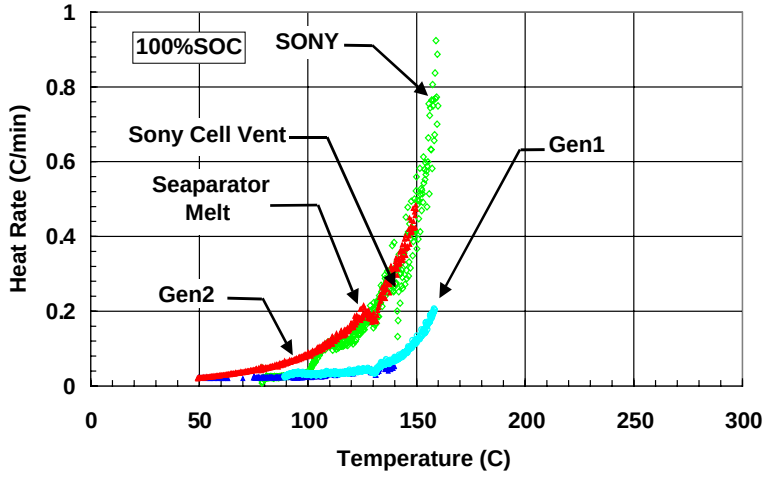

Fig. 6. Comparison of ARC data for Sony, Gen1 and Gen2 cells at 100% SOC.

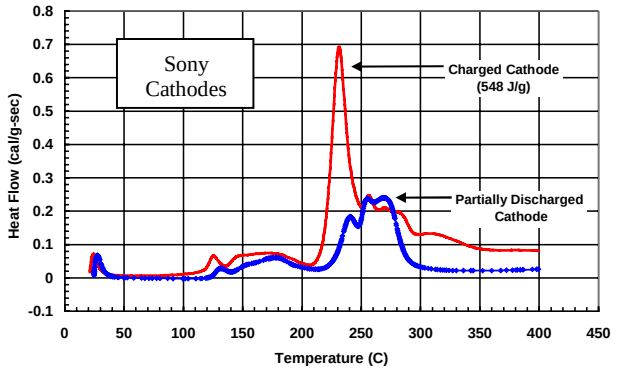

Fig. 8. DSC profiles of charged and discharged Sony cathodes in electrolyte.

EC:DEC (1:1) electrolyte. The discharged Gen1 anode material (MCMB) showed a sharp exothermic decomposition at 125 °C with no further reactions up to 400 °C as shown in Fig. 10. This sharp exotherm indicates the presence of a well-developed SEI layer on this MCMB carbon that undergoes exothermic decomposition as discussed previously. Since there is no intercalated lithium in the carbon particles, there are no further reactions with the electrolyte and binder materials. The charged anodes showed an exothermic onset at this temperature followed immediately by the exothermic reduction of the electrolyte by the lithiated carbon. The peak in this reaction occurs in the 250 °C to 300 °C range but was partially affected by the endothermic venting of the DSC pan.

The Gen1 cathode materials ($LiNi_{0.85}Co_{0.15}O_2$) were also measured in the charged and discharged states as shown in Fig. 11. The charged cathode showed a sharp exothermic peak at 225 °C while the discharged material showed a reduced exothermic peak shifted up to 260 °C. This cathode material did not show any exothermic activity below 200 °C.

The Gen1 fully charged anode and cathode materials are compared in Fig. 12. Initial thermal reactions occur at the anode but at a very low rate due to the well-developed SEI

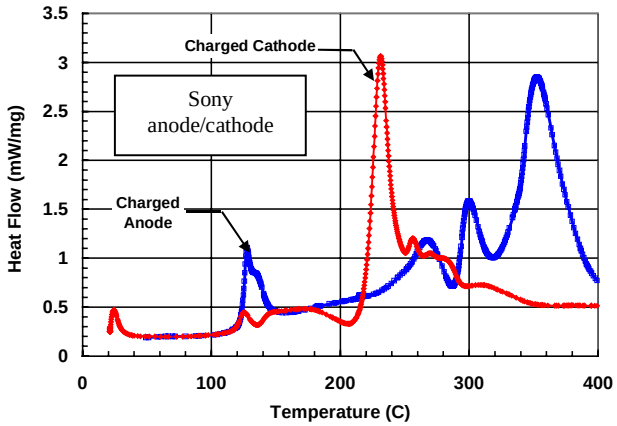

Fig. 9. DSC profiles of charged Sony anode and cathode material in electrolyte.

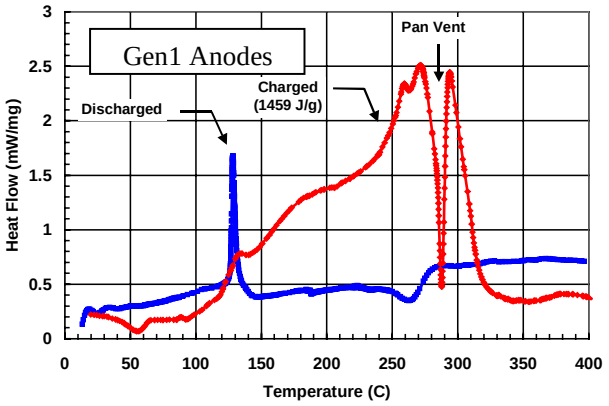

Fig. 10. DSC profiles of Gen1 charged and discharged anodes in 1 M $LiPF_6$ EC:DEC electrolyte.

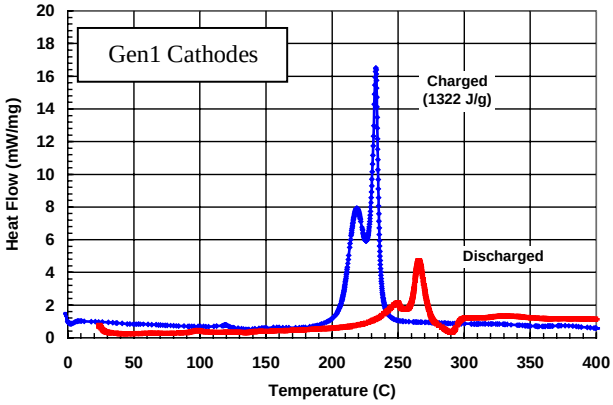

Fig. 11. DSC profile of charged and discharged Gen1 cathodes in 1 M $LiPF_6$ EC:DEC electrolyte.

layer. The first strong exothermic reaction occurs at the cathode followed by a lesser exothermic peak at the anode. This is the same sequence of reactions seen for the Sony materials except that the Sony anode showed a much sharper initial SEI decomposition reaction. Also, no high temperature reaction was seen in the Gen1 anodes above 300 °C.

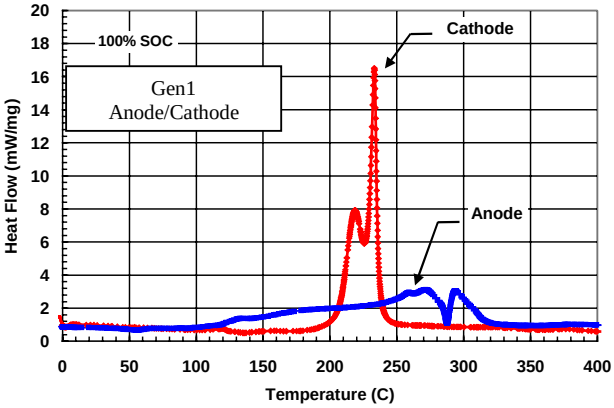

Fig. 12. DSC profiles of charged Gen1 anodes and cathodes in 1 M $LiPF_6$ EC:DEC electrolyte.

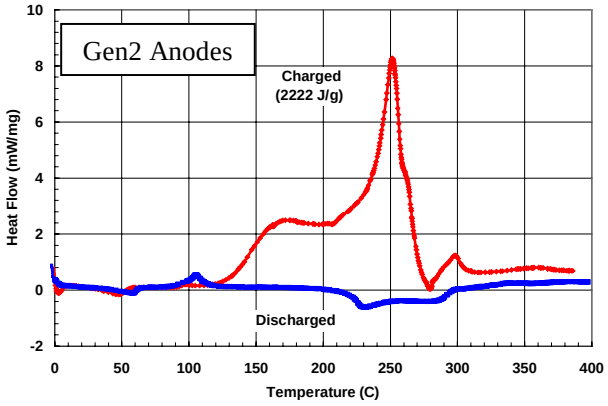

Fig. 13. DSC profiles of charged and discharged Gen2 anodes in 1 M $LiPF_6$ EC:DEC electrolyte.

3.2.3. Gen2 cells

Gen2 cells at 100 and 0% SOC were disassembled as done for the previous cells. DSC measurements were performed using the Gen2 1.2 M $LiPF_6$ EC:EMC (3:7) electrolyte. The DSC data for the charged/discharged anode materials are shown in Fig. 13. The discharged anode material showed a small SEI reaction centered at 100 °C while the charged material showed an even smaller SEI exotherm followed by a large electrolyte reduction exothermic region. The Gen2 anode material showed evidence of a very weak SEI layer compared to the Gen1 anodes.

The Gen2 cathodes, with the Al stabilized $LiNi_{0.80}Co_{0.15}Al_{0.05}O_2$, showed reaction peaks about 25 °C higher than seen for the Gen1 cathodes for both charged and discharged materials as shown in Fig. 14. Comparison of the anode and cathode materials in Fig. 15 shows that the reaction peak temperatures were very close and the magnitude of the reactions both were greater than seen for the Gen1 materials. The anode showed the lowest temperature onset of exothermic reaction followed by the sharp cathode exotherm as seen for the Sony and Gen1 materials.

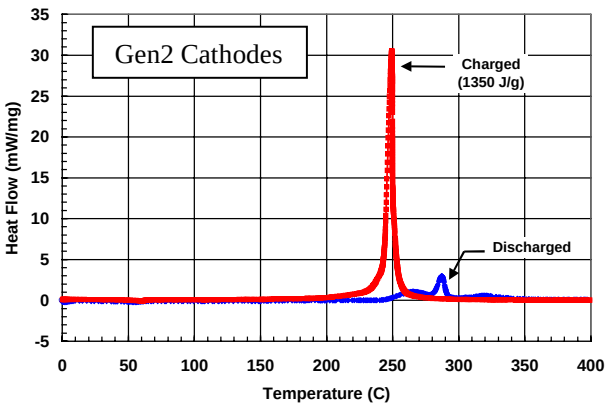

Fig. 14. DSC profiles of charged/discharged Gen2 cathodes in 1 M $LiPF_6$ EC:DEC electrolyte.

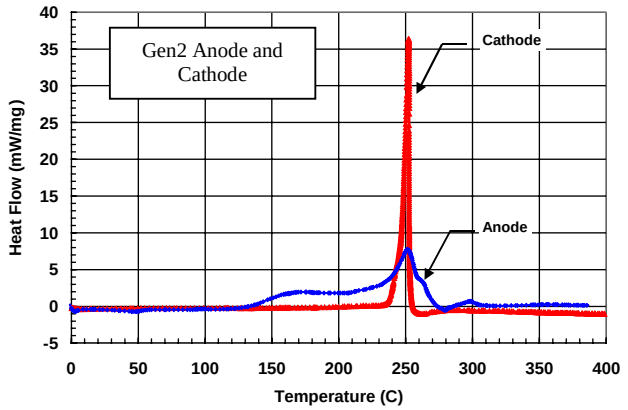

Fig. 15. DSC profile of charged Gen2 anodes and cathodes in 1 M $LiPF_6$ EC:DEC electrolyte.

3.2.4. Sony, Gen1 and Gen2 cell comparison

The anode materials for the Sony, Gen1 and Gen2 cells are compared in Fig. 16. The total reaction enthalpies calculated for each material showed that the highest enthalpy occurred for the Gen2 anodes with a value of 2222 J/g based on the film weight. The Gen1 anode had a value of 1459 J/g while the Sony anode showed an intermediate value of 1883 J/g. However, the Sony anode enthalpy up to 325 °C was only 416 J/g if the unknown high temperature exotherm is excluded for comparative purposes. The Sony anodes showed the most marked SEI decomposition reaction at 125 °C, which can account for the sudden onset of thermal runaway seen in the ARC data at that temperature. The Gen1 anodes showed a steady increase in the reaction rate while the Gen2 materials showed a much greater rate of increase also indicated by their ARC profiles. The nature of the graphite particles had a significant impact on the thermal decomposition response.

SEM micrographs taken of the anode films for the Gen1 and Gen2 materials are shown in Fig. 17 [12]. The Gen1 MCMB graphite shows a highly spherical particle structure while the Gen2 MAG10 graphite has flaky particles with

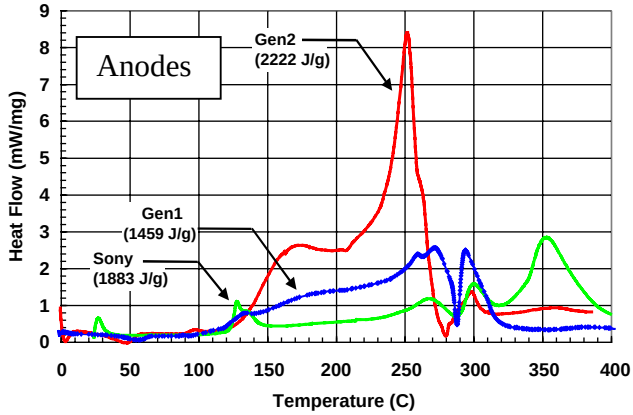

Fig. 16. DSC comparison of Sony, Gen1 and Gen2 charged anodes in electrolyte.

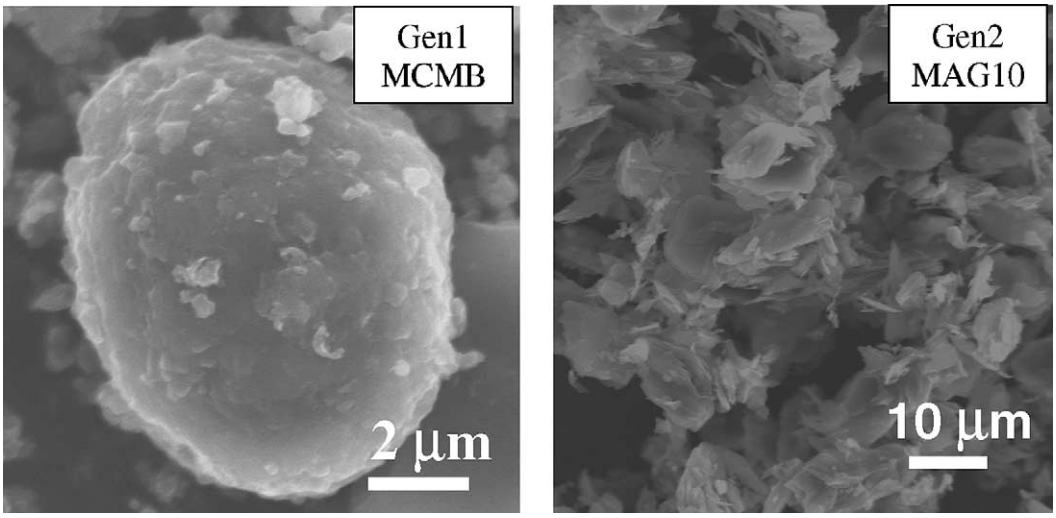

Fig. 17. SEM micrographs of Gen1 (MCMB) and Gen2 (MAG10) anode particles.

many edges. The calorimetric data indicate that the MCMB graphite particles form a highly effective SEI passivation layer that undergoes only gradual decomposition at elevated temperatures. The flaky Gen2 particles are not completely protected by the SEI layer, having many reactive edges still capable of reacting with the electrolyte [13].

The reaction enthalpies for the Gen1 and Gen2 cathodes were very similar, 1322 and 1350 J/g, respectively as shown in Fig. 18. However, the Al stabilized Gen2 cathode had a higher reaction onset temperature. Thus the greater thermal instability of the Gen2 cells resulted primarily from the more reactive anode particles. The Sony cathode material had a low reaction enthalpy of only 548 J/g with a similar peak reaction temperature as for the Gen1 cathodes.

An estimate of the contribution of each electrode component to the possible total cell reaction enthalpy is calculated in Table 2 for the Gen2 cells. This table gives the electrode masses, reactive component masses and reaction enthalpies of each major cell component for the Gen2 cells. The anode material is shown to have the highest contribution to the overall cell reaction but the cathode is of comparable magnitude. The free electrolyte contributes a maximum of 6% to the total reaction enthalpy and is certainly lower due to electrolyte reaction at lower temperatures with the active electrode materials.

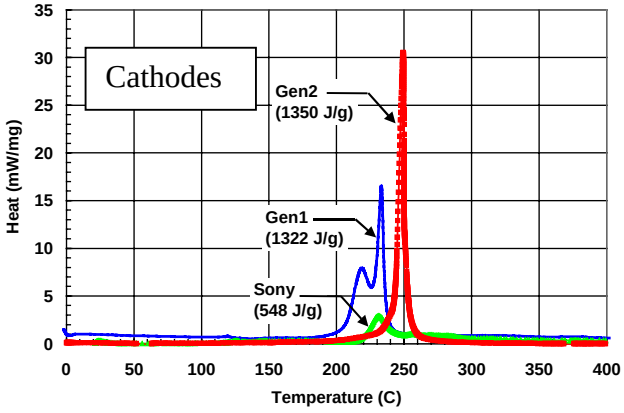

Fig. 18. DSC comparison of Sony, Gen1 and Gen2 charged cathodes in electrolyte.

3.2.5. *Effects of aging*

It has been shown that the SEI layer formed during initial lithiation transforms over time, forming a more inert layer [6,7]. The initial SEI layer changes from an organic layer to a more stable inorganic layer composed mostly of species such as Li_2CO_3 and LiF [14–18]. The LiF product results from reaction with HF in the electrolyte, which arises from reaction of the $LiPF_6$ with trace water. This new layer can affect the rate of thermal decomposition of the remaining SEI layer. We measured the effect of aging in the Sony, Gen1 and Gen2 cells after holding them for increasing periods at elevated temperatures and states of charge. ARC and DSC runs were performed on selected disassembled cells.

3.2.5.1. Sony cells. Fig. 19 shows the ARC data for the aged Sony cells (25–70 °C). These commercial Sony cells have an unknown history and thus “fresh” cells already have some aging effects in their thermal response. Cells maintained at room temperature for an additional 6 months showed an increase in the onset temperature for self-generated heating from 65 to 90 °C indicating that

Table 2
Gen2 cell component weights and reaction enthalpies

	Positive	Negative	Electrolyte	Cell
Weight (g)	10.68	12.07	5.49	37.8
Active weight (g)	6.5	5.2	5.49	
Heat of reaction (kJ/g)	1.35	2.22	0.22	
Enthalpy (kJ)	8.8	11.5	1.2	21.5
Reaction (%)	41	53	6	

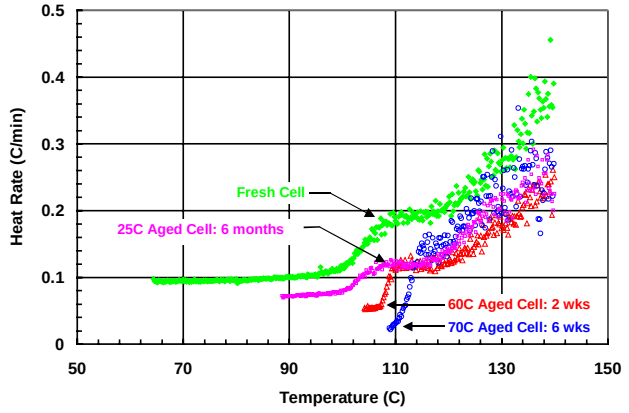

Fig. 19. ARC data for Sony cells with increased aging (vertically offset).

the SEI layer was continuing to evolve. However, with increased aging temperature and time the onset of this reaction continued to shift to higher temperatures. Aging of the "fresh" cells at 60 °C for only 2 weeks resulted in a shift in the onset temperature from 65 to almost 105 °C. However, cells aged at 70 °C for 6 weeks had only a relatively small additional increase in the onset temperature. A limit to the effectiveness of the SEI layer may be reached either due to reduced growth by diffusion through the increased layer thickness or by changes in the composition of the growing layer. All cells, regardless of aging, showed a "knee" in the heating rate around 110 °C followed by accelerating heating rate due to continued electrolyte reduction by the lithiated anode carbon. The Sony SEI layer apparently has a thermal stability limit independent of film thickness.

3.2.5.2. Gen1 cells. Fig. 20 shows ARC data for the Gen1 cells calendar aged at 40, 50 and 60 °C/80% SOC for 4 weeks. All aged cells showed a shift of the onset reaction temperature to higher temperatures as seen for the Sony cells. The cells aged at 40 °C showed a significant reduction in sustained heat generation below 140 °C. However, with aging at the higher temperatures of 50 and 60 °C the cells behaved similarly to the fresh cell. The only significant effect was the shift in the onset temperatures. Accelerating heating rates were seen for all cells above 140 °C with almost identical heating rates by 160 °C. These results suggest that the transformed SEI layer on the Gen1 anodes may be very delicate. Although the inorganic species such as LiF will not dissolve at these temperatures, the morphology of the layer may depend on aging temperature and the surface characteristics of the carbon particles. If the inorganic layer is discontinuous and cracked, the electrolyte can penetrate near to the carbon particle and intercalated Li can continue to react to form new SEI with the associated heat generation.

3.2.5.3. Gen2 cells. As part of the ATD program, an Accelerated Life Test study of the Gen2 cells was performed with cells subject to aging at elevated temperatures (25, 35, 45 and 55 °C) and states of charge (60, 80 and 100%). Selected cells from this test matrix were removed after aging and either measured in the ARC to determine changes in thermal runaway performance or disassembled for measurement of the individual electrode components.

A cell aged at 45 °C, 80% SOC for 8 weeks was measured in the ARC up to 150 °C. Fig. 21 shows the thermal runaway behavior of this cell compared to an unaged Gen2 cell both of which were measured at 100% SOC. Aging reduced the heating rate of the cell at any given temperature and increased the temperature of onset of self-generated heating as seen for the other cell chemistries. Venting of the cell occurred at 130 °C. The separator melt endotherm was also measured beginning at this temperature. No increase in heating rate was seen, indicating that the cell did not undergo any internal shorting resulting from the separator melt. All of the aged cells showed venting near this temperature indicating that increased gas formation occurred during the aging period.

A cell aged at 55 °C, 80% SOC for 20 weeks was disassembled to remove the electrode components for DSC analysis. Fig. 22 shows the data for the 20 week aged anode compared with the DSC data for the 8-week aged and an unaged anode all measured in the presence of Gen2 electrolyte. Aging resulted in reduced exothermic reactions and

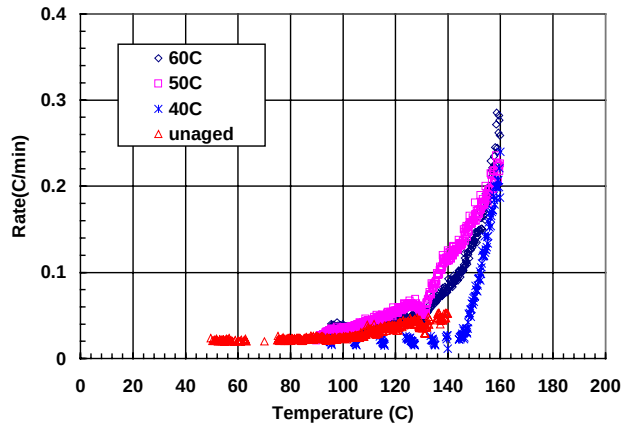

Fig. 20. ARC data for Gen1 cells with increased aging.

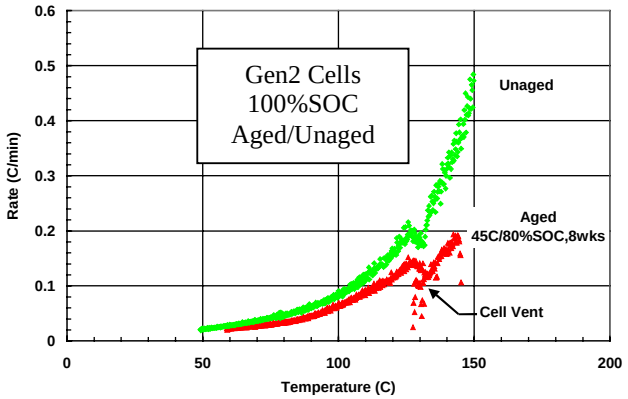

Fig. 21. ARC data of aged and unaged Gen2 cells at 100% SOC.

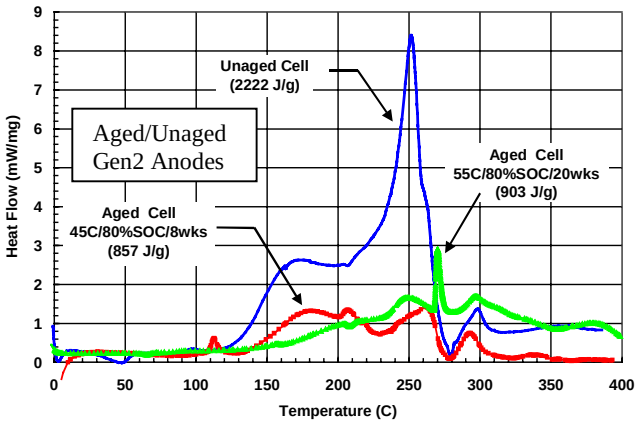

Fig. 22. DSC profiles of aged and unaged Gen2 anodes in 1 M $LiPF_6$ EC:DEC electrolyte.

increased temperatures for the onset of decomposition as was seen in the ARC data for the response of the full cell. During these accelerated aging periods, the anodes developed a thicker and more effective SEI layer that reduced the interaction between the lithiated carbon and the electrolyte. Integration of these exotherms showed that the heat of reaction decreased from 2222 J/g for the unaged anode to 857 and 903 J/g for the 8- and 20-week aged cells, respectively. The aged anodes showed comparable reaction enthalpies but with higher temperature of SEI decomposition for the more aged cell. The effects of aging occur quickly at the anodes but then progress at a comparably slow rate.

Fig. 23 shows a comparison of the DSC data for the cathode materials from the same cells. Initial aging during the 8 week period had little effect on the magnitude of the exotherm and the temperature of the reaction. The cathode of the cell aged at 55 °C for 20 weeks showed a similar reaction enthalpy, 1228 J/g, compared to 1287 J/g for the 8-week aged cathode. However, the reaction occurred over a broader temperature range and the peak reaction rate decreased for this more aged cathode. Aging at the cathode may be a more complex process involving not only formation of an SEI

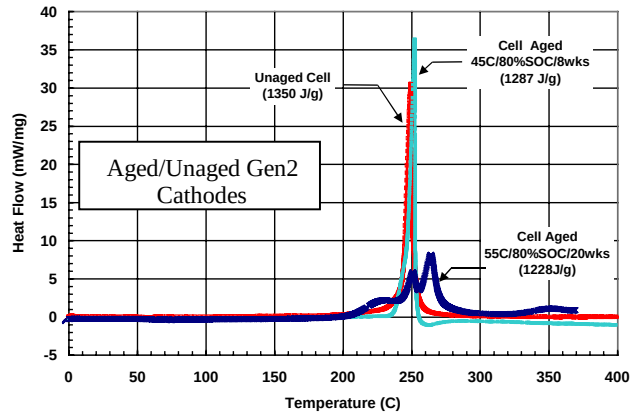

Fig. 23. DSC profiles of aged and unaged Gen2 cathodes in 1 M $LiPF_6$ EC:DEC electrolyte.

layer but changes in the properties of the oxide material that affect high-temperature decomposition and reactions [19].

4. Conclusions

High-power cells were developed for the ATD program and characterized for their abuse tolerance along with commercial Sony 18650 cells. The calorimetric methods of ARC and DSC were used to determine the thermal runaway response of these cells as a function of state of charge and aging. Individual cell components were measured to determine the contributing effects of the anode and cathode materials on overall cell thermal abuse performance.

For all cells, the initial heat generation began with the anode SEI decomposition reaction in the 100–120 °C range followed by increasing exothermic reaction resulting from reduction of the electrolyte by the lithiated carbon. A peak in the reaction rate occurred around 250 °C. This reaction was very sensitive to state of charge and showed no appreciable exothermic activity for fully discharged cells. Cathode reactions showed a sharp reaction peak in the 200–250 °C range and were also highly dependent on SOC. The cathodes showed higher peak reaction rates over narrower temperature range than was seen for the anode reactions.

The morphology of the anode carbon particles determined the thermal response of the anode film and the initial ARC thermal runaway profile. The spherical Gen1 MCMB carbon particles developed a stable SEI layer that decreased the ARC thermal runaway reaction. The Gen1 cells showed much greater thermal stability than was seen for the commercial Sony cells. The flaky Gen2 MAG10 carbon particles developed an ineffective SEI layer that allowed initiation of continuous thermal runaway as low as 50 °C, very similar to the performance of the Sony cells. Increasing SOC lowered the onset temperature for thermal runaway and increased the acceleration rate for all cells.

Aging at elevated temperature resulted in more thermally stable cells with higher onset temperature and reduced heating rate. The Gen2 anode material showed a rapid initial reduction in exothermic reactions with aging followed by a gradual shift in reaction temperatures to higher values with increased aging. The Gen2 cathode material showed a reduction in exothermic reaction only after extended aging.

The thermal abuse tolerance of Li-ion cells has been shown to be a sensitive function of the cell component properties. High-power cells can be designed for both performance and safety by the proper choice of cell materials based on an understanding of the contributing reaction mechanisms.

Acknowledgements

The authors wish to thank Bob Patton and GiGi Gonzales for the DSC and ARC measurements This work was

performed under the auspices of DOE FreedomCAR & Vehicle Technologies Office through the Advanced Technology Development (ATD) High Power Battery Development Program. Sandia is a multiprogram laboratory operated by Sandia Corporation, a Lockheed Martin Company, for the United States Department of Energy under Contract DE-AC04-94AL85000.

References

[1] S. Al Hallaj, H. Makeki, J.S. Hong, J.R. Selman, J. Power Sources 83 (1999) 1–8.
[2] J. Shi, C. Lampe-Onnerud, P. Ralbovsky, P. Onnerud, E. Carlson, B. Barnett, Electrochem. Soc. Proc. 98–16 (1998) 493–499.
[3] H. Maleki, G. Deng, A. Anani, J. Howard, J. Electrochem. Soc. 146 (9) (1999) 3224–3229.
[4] PolyStor Corp., 230 S. Vasco Road, Livermore, CA 94550, USA.
[5] Quallion LLC, P.O. Box 923127, Sylmar, CA 91392-3127, USA.
[6] M.N. Richard, J.R. Dahn, J. Electrochem. Soc. 146 (1999) 2068–2077.
[7] M.N. Richard, J.R. Dahn, J. Electrochem. Soc. 146 (1999) 2078–2084.
[8] Proceedings of LONG BEACH 2001: The 16th Annual Battery Conference on Applications and Advances by IEEE Aerospace and Electronic Systems Society, Long Beach, CA, 9–12 January 2001, 375–380.
[9] D.D. MacNeil, T.D. Hatchard, J.R. Dahn, J. Electrochem. Soc. 148 (2001) A663–A667.
[10] D.D. MacNeil, J.R. Dahn, J. Electrochem. Soc. 149 (2002) A912–A919.
[11] Y. Baba, S. Okada, J. Yamaki, Solid State Ionics 148 (2002) 311–316.
[12] SEM micrographs provided by Argonne National Laboratory, Argonne, IL.
[13] T. Zheng, A.S. Gozdz, G.G. Amatucci, J. Electrochem. Soc. 146 (11) (1999) 4014–4018.
[14] A.M. Andersson, K. Edstrom, N. Rao, A. Wendsjo, J. Power Sources 81–82 (1999) 286–290.
[15] A.M. Andersson, M. Herstedt, A.G. Bishop, K. Edstrom, Electochem. Acta 47 (2002) 1885–1898.
[16] D. Aurbach, Y. Ein-Ely, A. Zaban, J. Electrochem. Soc. 141 (1994) L1.
[17] T. Sato, M. Deschamps, H. Suzuki, H. Ota, H. Asahina, S. Mori, Mater. Res. Soc. Symp. Proc. 496 (1998) 457.
[18] C.R. Yang, Y.Y. Wang, C.C. Wan, J. Power Sources 72 (1998) 66–70.
[19] J. Shim, R. Kostecki, T. Richardson, X. Song, K.A. Striebel, J. Power Sources 112 (2002) 222–230.